DOI: 10.1021/ma901973t

Macromolecules
ARTICLE

Effect of Surface Molecular Aggregation State and Surface Molecular Motion on Wetting Behavior of Water on Poly(fluoroalkyl methacrylate) Thin Films

Koji Honda,[†] Masamichi Morita,[‡] Osami Sakata,[§] Sono Sasaki,[§] and Atsushi Takahara*[,†,⊥]

[†]*Department of Chemistry and Biochemistry, Graduate School of Engineering, Kyushu University, Motooka, Nishi-ku, Fukuoka 819-0395, Japan,* [‡]*Chemical R&D Center, Daikin Industries, Ltd., 1-1 Nishi Hitotsuya, Settsu-shi, Osaka 566-8585, Japan,* [§]*Japan Synchrotron Radiation Research Institute/SPring-8, Sayo, Hyogo 679-5198, Japan, and* [⊥]*Institute for Materials Chemistry and Engineering, Kyushu University, Motooka, Nishi-ku, Fukuoka 819-0395, Japan*

Received September 3, 2009; Revised Manuscript Received November 25, 2009

ABSTRACT: The effect of surface molecular motion on the wetting behavior of water on the thin film surfaces of poly(fluoroalkyl methacrylate)s with various fluoroalkyl (R_f) groups [PFMA-C_y; y: fluoromethylene number in R_f groups, y = 1, 2, 4, 6, and 8] was characterized. The receding contact angle of PFMA-C_y with short R_f groups (y = 1, 2, 4, and 6) was larger than that of poly(fluoroalkyl acrylate) with short R_f groups [PFA-C_y, $y \leq 6$]. This stable hydrophobicity observed for PFMA-C_y is due to the restriction of thermal molecular motion by the α-methyl group. Wide-angle X-ray diffraction (WAXD) and grazing incidence WAXD measurements revealed that the R_f groups [PFMA-C_y, $y \leq 6$] were not crystallized. PFMA-C_8 showed high advancing and receding contact angles due to the crystallization of fluoroalkyl groups at the surface region. The hydrophobicity of PFMA-C_8 was improved after annealing due to the ordering of fluoroalkyl groups.

Introduction

Polymers with fluoroalkyl (R_f) groups show surface characteristics that differ greatly from those of comparable hydrogenated polymers; examples of such characteristics are excellent chemical and thermal stability,[1] nonadhesive properties,[2] low surface free energies,[3] and low friction coefficients. Thus, these polymers have been extensively studied and utilized as important materials in industry for the production of various surface functional chemicals such as water repellents and oil repellents for textiles, surface modifiers for plastic, paper, and metal, and additives for lubrication and antifriction. Typical examples of these polymers are poly(fluoroalkyl acrylate)s with long R_f groups, and these polymers have a critical surface tension (γ_c) that is much lower than that of polytetraflouoroethylene (PTFE), which is a typical fluoropolymer.[3−7] Dow's group revealed that fluoroalkyl chain density and fraction of polar component were important factors determining hydrophobicity and nonstickiness.[2] However, the water-repellent mechanism of these polymers was not clarified on the basis of surface structure and surface molecular motion.

In the previous report, the authors clarified the water-repellent mechanism of poly(fluoroalkyl acrylate) (PFA-C_y, where y is the fluoromethylne number of the R_f groups) thin films.[8−12] In the case of PFA-C_y with long R_f groups [$y \geq 8$], the mobility of the side chains is low because of the crystallization of the R_f groups at the surface region; therefore, the decrease of the contact angle against water did not occur by surface reorganization upon exposure to water. Further, the authors recently tried to fabricate nanostructures for PFA-C_8 thin films by nanoimprinting lithography[13,14]—a technique in which a mold with a nanostructured surface pattern is mechanically pressed onto a substrate coated with polymeric materials. The authors discovered that a PFA-C_8 film could be nanoimprinted at room temperature.[13,14] It is possible to nanoimprint this crystalline film because of the presence of the oriented bilayer soft crystal without spherulite structure and the weak molecular interaction of R_f groups.

The mobility of molecular chains is an important factor in determining wetting behavior.[15,16] Katano et al. reported that PFA-C_8 and PFMA-C_8 film after heating and quenched in water showed different surface properties from the original one.[6] However, the relationship between the mobility of molecular chains and wetting behavior has not been evaluated directly. Since the bioaccumulation of the degraded product of perfluorinated acid with long fluoroalkyl chain ($C_n \geq 8$) is becoming a serious concern, it is necessary to design fluoropolymer coating with short fluoroalkyl chain.[17,18] One of the motivations of this study is to reveal the polymer design principle for high hydrophobicity with short fluoroalkyl side chains. In this study, the authors have investigated the effect of surface molecular motion on the wetting properties of thin films of poly(fluoroalkyl methacrylate)s with R_f groups [PFMA-C_y, y = 1, 2, 4, 6, and 8] and clarified the relationship between the surface molecular motion and wetting properties.

Experimental Section

1. Materials. *Polymerization.* The chemical structure of PFMA-C_y is shown in Chart 1. Fluoroalkyl methacrylate monomers were provided by Daikin Industries Co., Ltd. PFMA-C_y was prepared by radical polymerization under a nitrogen atmosphere in 3,3-dichloro-1,1,1,2,2-pentafluoropropane (HCFC-225) at 323 K for 18 h using azobisisobutyronitryl (AIBN) as an initiator.[19] All the polymers, except for PFMA-C_1, were purified by precipitation in methanol. PFMA-C_1 was precipitated in hexane. PFMA-C_y was obtained as a white powder.

*Corresponding author: Tel +81-802-2517, Fax +81-92-802-2518, e-mail takahara@cstf.kyushu-u.ac.jp.

 Published on Web 12/11/2009

Chart 1. Chemical Structure of Poly(fluoroalkyl methacrylate)s [PFMA-C_y, Where y is the Fluoromethylene Number of the Fluoromethylene Group] (x = 1 for y = 1 and 2, x = 2 for y = 4, 6, and 8)

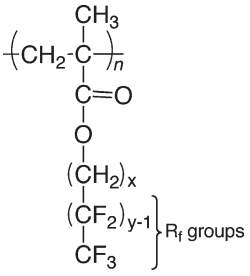

Preparation of Thin Polymer Films. PFMA-C_y was dissolved in HCFC-225 (concentration: 1 wt %), and a Si wafer was coated with this solution by the spin-coating method (2000 rpm, 30 s). The film thickness was estimated to be ~100 nm by a thickness measurement with atomic force microscopy (AFM). The AFM observation was performed using an SPA 4000 (SII-Nanotechnology Inc.). AFM images were obtained in the constant force mode in the air at 300 K using a 100 μm × 100 μm scanner and a Si_3N_4 tip on a triangle cantilever with a spring constant of 0.032 N m^{-1}. The films described in this paper were not annealed, unless mentioned otherwise.

2. Measurements. The wetting properties were evaluated by static and dynamic contact angle measurements. The crystalline states of PFMA-C_y were determined by wide-angle X-ray diffraction (WAXD) and grazing-incidence WAXD (GIWAXD) measurements. Thermal analysis was carried out by differential scanning calorimetry (DSC). The relationship between the wetting properties and the surface molecular motion was evaluated by temperature dependence of the dynamic contact angle, X-ray photoelectron spectroscopy (XPS), and lateral force microscopic (LFM) measurements.

Contact Angle Measurement. The static and dynamic contact angles were measured on a DSA-10 (Krüss Co., Ltd.). The static contact angles of water and methylene iodide (the volume of each was 2 μL) were measured, and the surface free energy was calculated from the static contact angles using the Owens and Wendt equation.[20] The dynamic contact angles were measured using an inclinable plane.[21] On the inclinable plane, a sample was placed on a stage, and the sample was tilted until a 50 μL water droplet began to slide down onto the sample. Subsequently, an advancing contact angle (θ_a), a receding contact angle (θ_r), and a sliding angle (θ_s) were determined. The contact angle hysteresis, $\Delta\theta$ ($= \theta_a - \theta_r$), is often a result of the surface reorganization and mobility.[22] The average of the five readings was used as the data.

DSC. The DSC curves were obtained using a DSC8230 (Rigaku Co., Ltd.). A 5 mg sample was heated at a heating rate of 10 K/min in an aluminum pan. Prior to performing the DSC measurements, the samples were preheated to 473 K to eliminate the effects of thermal history. Subsequently, the samples were cooled to 173 K, and then, measurements were performed in the temperature range 173−473 K.

WAXD. The WAXD measurements were carried out on a Rigaku RINT 2500 V (Rigaku Co., Ltd.) with a Cu Kα X-ray source (40 kV, 200 mA) for PFMA-C_y powder. The wavelength, λ, of the incident X-ray was 0.1542 nm. The data collection time was 3 s per step at 0.05° intervals. The scattering vector (q) was defined as $(4\pi/\lambda) \sin\theta$.

GIWAXD. GIWAXD measurements were carried out for the films at 300 K using a six-axis diffractometer installed at a BL-13XU beamline in SPring-8 (Japan Synchrotron Radiation Research Institute, Hyogo, Japan)[23] for the spin-coated thin films of PFMA-C_8. The value of λ was equal to 0.1025 nm. The data collection time was 1.5 s per step, and the angular interval between steps was 0.05°. Figure 1 shows the schematic geometry

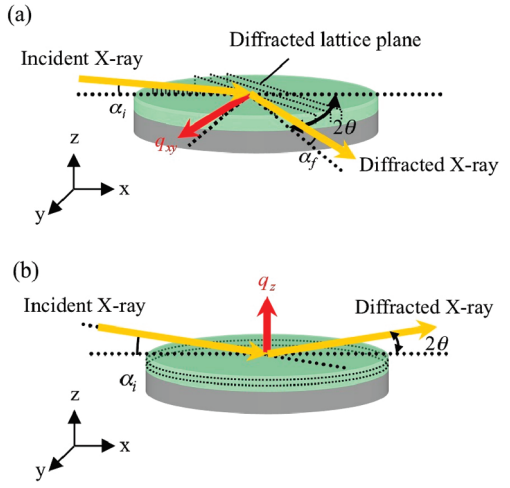

Figure 1. Schematic geometry of (a) in-plane and (b) out-of-plane GIWAXD measurements.

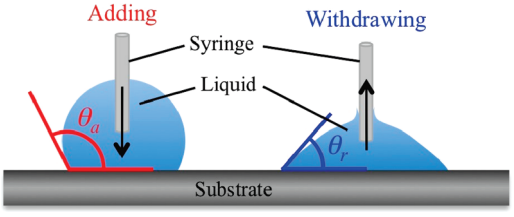

Figure 2. Schematic representation of dynamic contact angle measurement (θ_a: advancing contact angle; θ_r: receding contact angle).

of the in-plane and out-of-plane GIWAXD measurements. When the incident angle, α_i, is equal to or smaller than the critical angle, α_c, the incident X-rays undergo total external reflection and penetrate the samples as evanescent waves. For the present experimental conditions, α_c was calculated to be 0.100°. Thus, Bragg diffraction was observed at the surface regions at α_i = 0.08°.[24] In the in-plane geometry, the scattering vector (q_{xy}) is parallel to the surface, and the detected diffraction profiles contain information on the crystalline structure perpendicular to the film surface. On the other hand, the information on the crystalline structure parallel to the surface is obtained from the out-of-plane geometry.

Temperature Dependences of Dynamic Contact Angle. The temperature dependence of the dynamic contact angle was performed in the temperature range 278−363 K with a DSA-10 installed in a heating and cooling chamber. The temperature was increased in steps of 5 K and kept constant for 10 min; then, the dynamic contact angle was measured by the controlled drop method (Figure 2).[25,26] In this method, θ_a and θ_r could be obtained by increasing or decreasing the volume until the three-phase boundary moved over the surface.

Temperature Dependence of Lateral Force. In order to evaluate the surface molecular motion of PFMA-C_y thin films, the LFM (E-Sweep, SII-Nanotechnology Inc.) measurements were carried out at various temperatures in the vacuum. The LFM is a useful tool for the measurement of lateral force. The lateral force is the sum of the frictional and adhesion forces acting between the sample surface and cantilever tip. Since the frictional force reflects the relaxation behavior of polymeric materials, it is possible to investigate the state of surface molecular motion.[27−30] A piezoscanner was thermally insulated from the heating stage. A Si_3N_4 tip that was integrated on a rectangular cantilever with a spring constant of 0.11 N m^{-1}, which was coated with gold, was used. The normal force applied on the cantilever tip was set as 1.0 nN. The scanning rate was 1 μm/s. The scratching of the surface was negligible under this scanning condition.

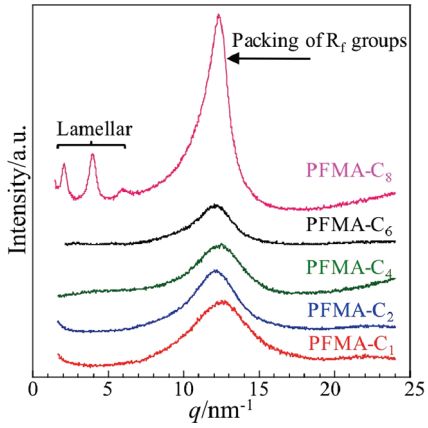

Figure 3. Powder diffraction profiles of PFMA-C_y. The λ of incident X-ray was 0.1542 nm.

Temperature Dependence of the Chemical Composition in the Surface Region. The XPS measurements were carried out on APEX (Ulvac Phi Inc.) with an Al Kα X-ray source. The X-ray gun was operated at 14 kV and 200 mA, and the analyzer chamber pressure was $10^{-9}-10^{-10}$ Pa. The take-off angles were kept constant at 45°. The samples were measured in the quickly dried from hydrated state to estimate the surface chemical composition in water.[31−35] The samples were hydrated by immersion in water (T = 298, 303, 313, 323, 333, 343, 353, and 363 K) for 120 min and then dried under vacuum (60 Pa) for 120 min, and then XPS measurements were performed. Since dring temperature is below T_g of the PFMA-C_y, the surface composition in the hydrated state might be kept during XPS measurement. Using the surface in a dried state as a reference, we defined rearrangement as the change from a hydrated surface composition to a dried one.

Results and Discussion

WAXD and DSC Measurements. Figure 3 shows the powder WAXD profiles of PFMA-C_y. The PFMA-C_y with $y \leq 6$ showed no sharp crystal diffraction peak. In the case of PFMA-C_8, crystalline diffraction peaks were obtained at q = 1−7 and 12.3 nm^{-1}. The peaks at q = 1−7 nm^{-1} were assignable to the lamellar structure in which the R_f groups were ordered like a multilayer,[36−38] and the peaks at q = 12.3 nm^{-1} were assignable to the packing of R_f side chains.[38,39] Table 1 lists the glass transition temperature (T_g) and the melting temperature (T_m) of PFMA-C_y and PFA-C_y measured by DSC. The T_m of side-chain crystallites was observed at 368 K for PFMA-C_8.[37,40] The higher melting point of PFMA-C_8 than PFA-C_8 can be attributed to the rigidity of main chain due to the presence of α-methyl group. In contrast, the measured values of T_g were 351, 343, 310, and 300 K for the PFMA-C_y with y = 1, 2, 4, and 6, respectively. These results were almost the same as those for PFA-C_y. However, the values of the T_g of the PFMA-C_y with $y \leq 6$ were higher than room temperature, while the values of the T_g of the PFA-C_y with $y \leq 6$ were lower than room temperature. This result indicates that the PFMA-C_y with $y \leq 6$ was in a glassy state at room temperature, and the mobility of the R_f groups was not activated at room temperature. The previous study suggested that the mobility of the molecular chain affects the wetting properties. Thus, it is expected that the wetting properties of PFMA-C_y with $y \leq 6$ are different from those of PFA-C_y.

Contact Angle Measurements for PFMA-C_y with $y \leq 6$. The results for the static contact angle against water and methylene iodide, surface free energy, and dynamic contact angle against water for the PFA-C_y and PFMA-C_y thin films

Table 1. Glass Transition Temperature (T_g) and Melting Temperature (T_m) of PFA-C_y and PFMA-C_y

sample	T_g/K	T_m/K
PFA-C_1	271	
PFA-C_2	259	
PFA-C_4	249	
PFA-C_6	243	
PFA-C_8		348
PFMA-C_1	351	
PFMA-C_2	343	
PFMA-C4	310	
PFMA-C_6	300	
PFMA-C_8		360

are summarized in Table 2. In the case of the PFMA-C_y with $y \leq 6$, the static contact angle and advancing contact angle (θ_a) were high, independent of the length of the R_f groups. These results were the same as those for the PFA-C_y. On the other hand, the receding contact angle (θ_r) was also large for the PFMA-C_y with $y \leq 6$, while it was small for the PFA-C_y with $y \leq 6$ ($< 50°$). Moreover, the sliding contact angle for the PFMA-C_y with ≤6 was small because of low magnitude of $\Delta\theta$.[41−44] These results indicate that for the PFMA-C_y with $y \leq 6$ the surface reorganization by exposure to water is hard to occur. In the case of PFA-C_y, the mobility of the molecular chains was active compared with that of PFMA-C_y because of the lack in crystallinity of the short R_f groups and the absence of α-methyl group which increases the flexibility of the main chain. This causes the decrease of the contact angle against water by surface reorganization. For PFMA-C_y, the WAXD measurements revealed that short R_f groups were not crystallized. However, the DSC measurements revealed that the main chain motion was not activated at room temperature ($\leq T_g$). These results suggest that the molecular motion of the main chains was not activated due to the presence of α-methyl groups and that the surface molecular motion of the R_f groups in the PFMA-C_y with $y \leq 6$ was also restricted by the relatively rigid main chains; further, it was difficult for the reorientation of the short R_f groups to occur at room temperature. Here, to evaluate the relationship between the surface molecular motion and wetting properties, the temperature dependence of the dynamic contact angle, XPS, and LFM measurements were carried out.

Relationship between Surface Molecular Motion and Wetting Properties for PFMA-C_y ($y \leq 6$). Figure 4 shows the temperature dependence of θ_r (red circles) and the lateral force (blue squares) for (a) PFMA-C_1, (b) PFMA-C_2, (c) PFMA-C_4, and (d) PFMA-C_6 thin films. At room temperature, θ_r showed high value as well as results measured using an inclinable plane. However, with an increase in temperature, for the PFMA-C_y thin films with y = 1, 2, 4, and 6, θ_r began to decrease drastically at 353, 343, 313, and 300 K, respectively. These temperatures approximately agreed with T_g values determined by DSC (green broken-dash arrows). Thus, it was considered that the decrease in θ_r was caused by the molecular motion activated above T_g. Here, the T_g determined by DSC is one of the bulk properties and not surface properties. Then, the temperature dependence of the LFM measurements was carried out in order to evaluate the surface molecular motion of PFMA-C_y thin films.

As shown in Figure 4, onset of an increase in lateral force was observed at 353, 346, 313, and 298 K for the PFMA-C_y with y = 1, 2, 4, and 6, respectively, and these temperatures could be empirically defined to be the surface T_g. These surface T_g's are located at the similar temperature to that of bulk T_g. Moreover, these surface T_g values showed good agreement with the temperature at which θ_r began to

Table 2. Static Contact Angle against Water (2 μL) and Methylene Iodide (CH_2I_2, 2 μL), Surface Free Energy (γ_s^d: Dispersion Force Component; γ_d^p: Polar Component; γ_s: Surface Free Energy), and Dynamic Contact Angle against Water (50 μL; θ_a: Advancing Contact Angle; θ_r: Receding Contact Angle; θ_s: Sliding Angle) for PFA-C_y and PFMA-C_y Films (*: Annealed at 333 K for 6 h)

	static contact angle/deg		surface free energy/mJ m^{-2}			dynamic contact angle/deg		
sample	water	CH_2I_2	γ_s^d	γ_s^p	γ_s	θ_a	θ_r	θ_s
PFA-C_1	102 ± 0.9	98 ± 4.0	7.52	5.10	12.62	106 ± 5.6	45 ± 2.5	48 ± 3.0
PFA-C_2	110 ± 3.9	100 ± 5.9	7.26	2.34	9.60	129 ± 6.5	48 ± 4.5	62 ± 2.5
PFA-C_4	126 ± 4.1	101 ± 5.3	8.44	0.04	8.48	132 ± 3.6	52 ± 3.0	58 ± 1.0
PFA-C_6	123 ± 4.9	103 ± 4.4	7.35	0.25	7.60	134 ± 4.0	52 ± 2.4	62 ± 3.4
PFA-C_8	122 ± 0.9	103 ± 0.4	7.46	0.36	7.83	126 ± 0.7	98 ± 2.6	20 ± 1.1
PFA-C_8*	121 ± 0.5	104 ± 1.0	6.84	0.59	7.43	125 ± 0.6	100 ± 1.5	19 ± 1.0
PFMA-C_1	94 ± 0.7	73 ± 1.9	19.1	3.8	22.9	102 ± 0.7	84 ± 0.8	14 ± 0.8
PFMA-C_2	106 ± 1.6	83 ± 0.7	14.7	1.5	16.2	111 ± 0.5	90 ± 1.0	15 ± 0.7
PFMA-C_4	114 ± 0.9	102 ± 1.9	7.22	1.60	8.82	120 ± 1.9	80 ± 1.5	28 ± 1.7
PFMA-C_6	117 ± 1.2	100 ± 0.9	8.21	0.91	9.12	120 ± 1.7	76 ± 2.7	31 ± 2.8
PFMA-C_8	118 ± 0.6	103 ± 2.0	7.00	1.02	8.02	123 ± 1.5	90 ± 1.5	22 ± 3.2
PFMA-C_8*	120 ± 0.7	105 ± 0.9	6.42	0.80	7.22	122 ± 1.3	112 ± 2.8	7 ± 1.5

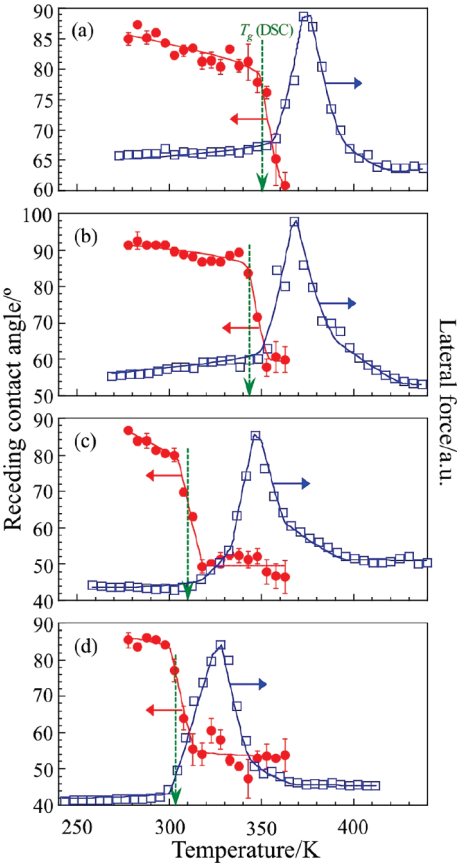

Figure 4. Temperature dependences of the receding contact angle (red circles) and lateral force (blue squares) for (a) PFMA-C_1, (b) PFMA-C_2, (c) PFMA-C_4, and (d) PFMA-C_6 thin films. Green broken dashed arrows indicate T_g determined from DSC measurement.

decrease. The authors already reported the surface T_g reduction of PS by temperature-dependent LFM.[28,30] However, this PFMA-C_y did not show the large decrease in T_g at the surface region. This is because the chain end localization at the surface did not occur because the fluoroalkyl side chain end groups had lower surface energy than main-chain end groups. The relationships between the onset of change in contact angle and T_g of PFMA-C_y indicate that the molecular motion greatly influences the wetting behavior. Below T_g, the surface molecular motion of the main chain is influenced by the α-methyl group, and it is difficult for surface reorganization to occur. On the other hand, above T_g, the surface molecular motion of the main chain and R_f group is activated in both surface and bulk, and the contact angle decreases easily by surface reorganization after exposure to water. Then, to confirm the surface reorganization by contacting water, the temperature dependence of the change in the chemical composition in the surface region was evaluated by XPS measurements.

Figure 5 shows the F_{1s}/C_{1s} and O_{1s}/C_{1s} values of (a) PFMA-C_1, (b) PFMA-C_2, (c) PFMA-C_4, and (d) PFMA-C_6 thin films in the dried and quickly dried from hydrated states. The F_{1s}/C_{1s} and O_{1s}/C_{1s} values represent the ratio of F and O atomic concentrations at the surface. In the case of dried state, the F_{1s}/C_{1s} and O_{1s}/C_{1s} values completely agreed with the theoretical values, which are calculated from the chemical structure of PFMA-C_y. In the quickly dried from hydrated state, below T_g, the F_{1s}/C_{1s} and O_{1s}/C_{1s} values did not show large change. On the other hand, above T_g, the F_{1s}/C_{1s} values decreased and the O_{1s}/C_{1s} values increased. The low values of F_{1s}/C_{1s} and the high values of O_{1s}/C_{1s} are probably because of the surface reorganization with exposure of carbonyl groups to the water interface. Hence, these results also support the relationship between the surface molecular motion and the wetting behavior of PFMA-C_y thin films.

Contact Angle Measurement for PFMA-C_8. From the powder WAXD and DSC measurements, it was revealed that PFMA-C_8 forms crystalline structures (Figure 3 and Table 1). Therefore, it is expected that the mobility of the R_f groups in PFMA-C_8 is very low and the water repellency is higher than that of the PFMA-C_y with $y \leq 6$. However, the θ_r of PFMA-C_8 was close to that of the PFMA-C_y with $y \leq 6$ (Table 2), and θ_r increased after annealing treatment (333 K for 6 h). Here, to discuss the effect of annealing treatment on the PFMA-C_8 thin film, the GIWAXD profiles before and after annealing (at 333, 348, and 368 K for 6 h) were compared.

Molecular Aggregation Structure of PFMA-C_8. There are several reports on the bulk and surface molecular aggregation states of polymer with fluoroalkyl side chains.[37,38,45,46] These reports seem to suggest that the connecting bond between fluoroalkyl side chain and main chain plays an important role for ordering of fluoroalkyl chains. Also, the preparation method and thermal history seem to influence the molecular aggregation states. In this study, the molecular aggregation states near the surface parallel and perpendicular directions were studied by GIWAXD. Figure 6 shows the (a) in-plane and (b) out-of-plane GIWAXD profiles measured at the surface region of the PFMA-C_8 thin films. In the in-plane and out-of-plane GIWAXD profiles, peaks were observed at $q_{xy} = 12.3\ nm^{-1}$ and $q_z = 1-7\ nm^{-1}$; these two peaks were assignable to the packing of the R_f groups and lamellar structures, respectively. Further, after annealing,

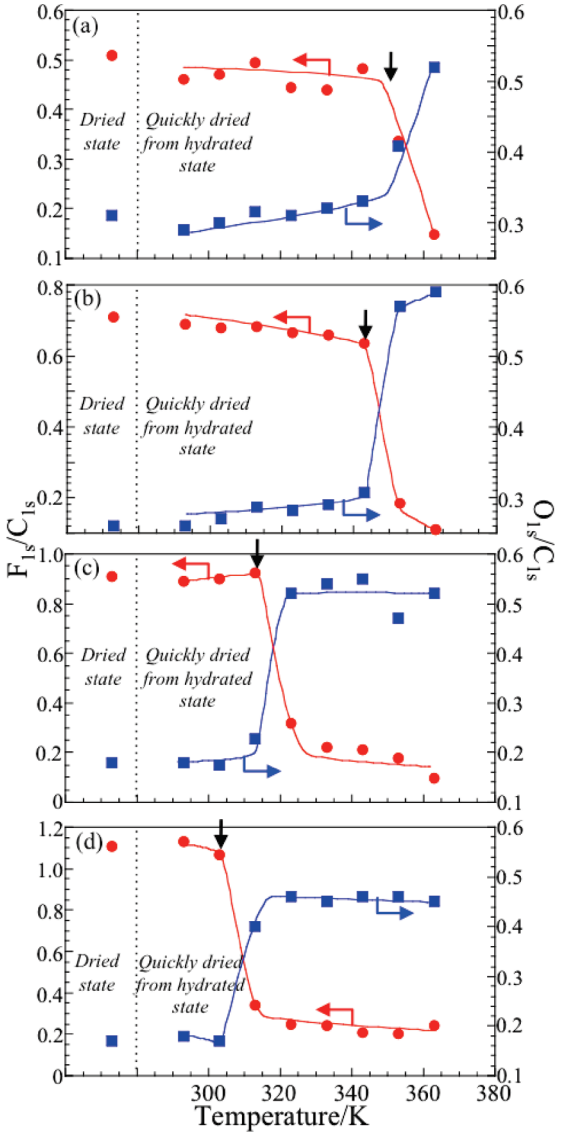

Figure 5. Temperature dependence of F_{1s}/C_{1s} and O_{1s}/C_{1s} values evaluated from XPS for PFMA-C_y thin films: (a) PFMA-C_1, (b) PFMA-C_2, (c) PFMA-C_4, and (d) PFMA-C_6 thin films.

the peaks became sharp and increased in intensity. These results indicate that the R_f groups and the lamellar structures are oriented perpendicular and parallel to the film surface, respectively, and that both the orientation and the order of the R_f groups improved as same as PFA-C_y with $y \geq 8$ thin films. In the case of PFA-C_8, θ_r did not change after annealing, though the peaks became sharper with an increase in the annealing temperature. Then, to evaluate the difference between PFA-C_8 and PFMA-C_8, the distortion of the crystalline lattice was estimated by applying the paracrystalline theory proposed by Hosemann.[47−49] In the paracrystalline lattice model, the lattice vectors of adjacent unit cells vary in magnitude and direction due to large displacements of the lattice points from their ideal positions, resulting in a loss of the long-range crystallographic order. Assuming that the form of the distribution function of the coordination statistics for the paracrystalline lattice model is identical to that of a Gaussian distribution, the paracrystalline lattice factor $Z(s)$ of the hth-order reflection is defined as

$$Z(s) = Z(h) = [1 - \exp(-4\pi^2 g^2 h^2)]/[(1 - \exp(-2\pi^2 g^2 h^2))^2 + (4 \sin^2 2\pi h) \exp((-2\pi^2 g^2 h^2)) \quad (1)$$

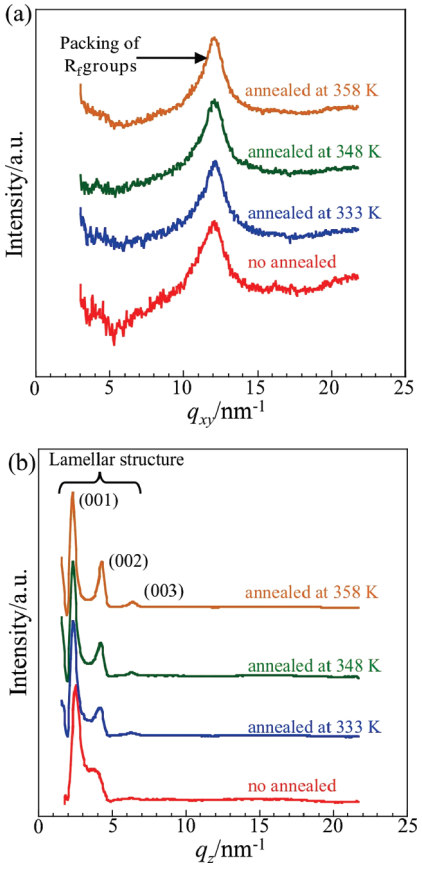

Figure 6. (a) In-plane and (b) out-of-plane GIWAXD profiles measured at surface region of PFMA-C_8 thin films. PFMA-C_8 films were annealed at 333, 348, and 358 K for 6 h. The λ of incident X-ray was 0.100 nm.

where s is the reciprocal lattice vector and g is the standard deviation of the Gaussian distribution divided by the average lattice vector $\tilde{a}$; g is a parameter that can be used to evaluate the degree of paracrystalline disorder. The integral width of a reflection is given by the value of g, which is experimentally given by

$$(\delta\beta)^2 = (1/\tilde{a}^2)[(1/N^2) + \pi^4 g^4 h^4] \quad (2)$$

Here, $\delta\beta$ is the integral breadth of a reflection, h is the scattering order, and N is the number of scattering units. Figure 7a shows a plot of $(\delta\beta)^2$ as a function of h^4 for the (001), (002), and (003) reflections on the PFMA-C_8 thin films. The least-squares fitting method gave a linear relation between $(\delta\beta)^2$ and h^4. The value of g was calculated using eq 2. Figure 7b shows the dependence of g on the annealing temperature for PFMA-C_8 and PFA-C_8 (the g for PFA-C_8 is cited from ref 10). As the annealing temperature increased, the value of g decreased from 7.5×10^{-3} to 4.2×10^{-3}, indicating that the paracrystalline distortion decreased and that both the orientation and order of the R_f groups improved. Here, the value of g for PFMA-C_8 was much larger than that for PFA-C_8 before annealing, and these values got closer after annealing. In the case of PFA-C_8, the orientation and ordering of the R_f groups before annealing is sufficiently high for achieving high water repellency. On the other hand, for PFMA-C_8, the orientation and ordering of the R_f groups before annealing is not high (Figure 8). As a result, before annealing, the θ_r of PFMA-C_8 is not higher than that of the PFMA-C_y with $y \leq 6$. The slight disordering of the R_f groups of PFMA-C_8 before annealing was probably caused by the α-methyl group. This behavior is similar to that observed for

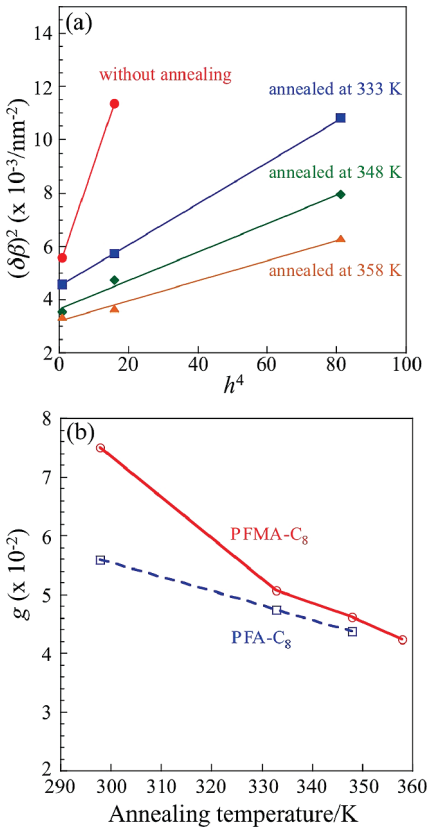

Figure 7. (a) Plot of $(\delta\beta)^2$ as a function of h^4 for the (001), (002), and (003) reflections of PFMA-C_8 thin films and (b) the annealing temperature dependence of g for PFMA-C_8 and PFA-C_8 (the data of PFA-C_8 are cited from ref 10).

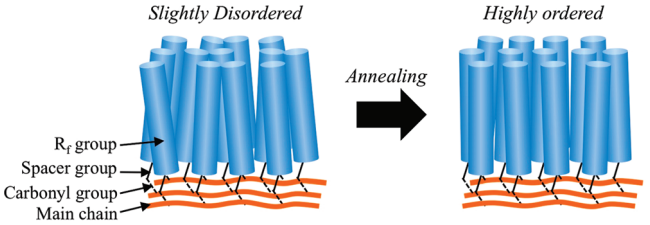

Figure 8. Schematic representation of the effect of annealing treatment on surface molecular aggregation state of PFMA-C_8 thin films.

poly(alkyl methacrylate)s.[50] After annealing, the R_f groups ordered closely and the water repellency increased.

Conclusions

The surface molecular aggregation states and surface properties of PFMA-C_y thin films were evaluated by dynamic contact angle, XPS, WAXD, GIWAXD, and LFM measurements. The relatively high magnitude of receding contact angle and low contact angle hysteresis on the PFMA-C_y film with short R_f groups (y = 1, 2, 4, and 6) was observed even though in the absence of crystallinity of R_f groups. This is because the T_g of PFMA-C_y is above room temperature owing to the reduction of molecular mobility due to the presence of α-methyl groups. This water repellent mechanism was also supported by the temperature dependence of the dynamic contact angle, surface composition, and lateral force. Advancing and receding contact angles of PFMA-C_8 were highest among PFMA-C_y with $1 \le y \le 6$ because of the surface crystallization of R_f groups. Moreover, GIWAXD measurements revealed that after annealing treatment the R_f groups in PFMA-C_8 became ordered and regular. These results suggest that the close packing of the R_f groups with y = 8 was inhibited by the rigid main chains before annealing treatment, and after annealing treatment, the R_f groups became ordered and the water repellency improved.

Acknowledgment. The present work was supported by a Grant-in-Aid for the Global COE Program, "Science for Future Molecular Systems" from the Ministry of Education, Culture, Science, Sports, and Technology of Japan. K.H. acknowledges the financial support of Grant-in-Aid for JSPS Fellows. The synchrotron radiation GIWAXD measurements were performed at the BL13XU in the SPring-8 with the approval of the Japan Synchrotron Radiation Research Institute (JASRI) (Proposal No. 2008B1498).

References and Notes

(1) Pittman, A. G. In *Fluoropolymers*; Wall, L. A., Ed.; Wiley-Interscience: New York, 1972; p 419.
(2) Schmidt, D. L.; Coburn, C. E.; Dekoven, B. M.; Potter, G. E.; Meyers, G. F.; Fischer, D. A. *Nature* **1994**, *368*, 39. Schmidt, D. L.; Dekoven, B. M.; Coburn, C. E.; Potter, G. E.; Meyers, G. F.; Fischer, D. A. *Langmuir* **1996**, *12*, 518.
(3) Sharfrin, E. G.; Zisman, W. A. *J. Phys. Chem.* **1960**, *64*, 519.
(4) Bernent, M. K.; Zisman, W. A. *J. Phys. Chem.* **1962**, *66*, 1207.
(5) Pittman, A. G.; Ludwig, B. A. *J. Polym. Sci., Part A1* **1969**, *7*, 3053.
(6) Katano, Y.; Tomono, H.; Nakajima, T. *Macromolecules* **1994**, *27*, 2342.
(7) Morita, M.; Ogisu, H.; Kubo, M. *J. Appl. Polym. Sci.* **1999**, *73*, 1741.
(8) Honda, K.; Morita, M.; Otsuka, H.; Takahara, A. *Macromolecules* **2005**, *38*, 5699.
(9) Honda, K.; Yakabe, T.; Koga, T.; Sasaki, S.; Sakata, O.; Otsuka, H.; Takahara, A. *Chem. Lett.* **2005**, *34*, 1024.
(10) Honda, K.; Morita, M.; Sasaki, S.; Sakata, O.; Takahara, A. *Trans. Mater. Res. Soc. Jpn.* **2006**, *32*, 239.
(11) Honda, K.; Morita, M.; Takahara, A. *Kobunshi Ronbunshu* **2007**, *64*, 181.
(12) Honda, K.; Yamaguchi, H.; Kobayashi, M.; Morota, M.; Takahara, A. *J. Phys. Conf. Ser.* **2008**, *100*, 012035.
(13) Honda, K.; Morita, M.; Takahara, A. *Soft Matter* **2008**, *4*, 1400.
(14) Honda, K.; Morita, M.; Masunaga, H.; Sasaki, S.; Takata, M.; Takahara, A. *Soft Matter*, DOI: 10.1039/B918316G.
(15) Kajiyama, T.; Teraya, T.; Takahara, A. *Polym. Bull.* **1990**, *24*, 333.
(16) Teraya, T.; Takahara, A.; Kajiyama, T. *Polymer* **1990**, *31*, 1149.
(17) http://www.fluoridealert.org/pesticides/pfoa.us.epa.fact.sheet.2003.pdf.
(18) Suja, F.; Pramanik, B. K.; Zain, S. M. *Water Sci. Technol.* **2009**, *60*, 1533.
(19) Shimizu, T. In *Modern Fluoropolymers*; Scheirs, J., Ed.; John Wiley & Sons: New York, 1997; p 507.
(20) Owens, D. K.; Wendt, R. C. *J. Appl. Polym. Sci.* **1969**, *13*, 1741.
(21) Extrand, C. W.; Kumagai, Y. *J. Colloid Interface Sci.* **1997**, *191*, 378.
(22) Takahara, A. In *Modern Approaches to Wettability: Theory and Applications*; Schrader, M. E., Loeb, G., Eds.; Plenum Press: New York, 1992; p 179.
(23) Sakata, O.; Furukawa, Y.; Goto, S.; Mochizuki, T.; Uruga, T.; Takeshita, K.; Ohashi, H.; Matsushita, T.; Takahashi, S.; Tajiri, H.; Ishikawa, T.; Nakamura, M.; Ito, M.; Sumitani, K.; Takashi, T.; Simura, T.; Saito, A.; Takahashi, M. *Surf. Rev. Lett.* **2003**, *10*, 543.
(24) Russell, T. P. *Mater. Sci. Rep. B.* **1989**, *5*, 171.
(25) Bartell, F. E.; Bjorklund, C. W. *J. Phys. Chem.* **1952**, *56*, 453.
(26) Johnson, R. E.; Dettre, R. H. In *Surface and Colloid Science*; Matijevic, E., Ed.; John Wiley & Sons: New York, 1969; p 85.
(27) Johnson, J. L.; Kendall, K.; Roberts, A. D. *Proc. R. Soc. London A* **1971**, *324*, 301.
(28) Kajiyama, T.; Tanaka, T.; Takahara, A. *Macromolecules* **1995**, *28*, 3482.
(29) Hammerschmidt, J. A.; Gladfelter, W. L.; Haugstad, G. *Macromolecules* **1999**, *32*, 3260.
(30) Tanaka, K.; Takahara, A.; Kajiyama, T. *Macromolecules* **2000**, *33*, 7588.
(31) Ratner, B. D.; Weathersby, P. K.; Hoffman, A. S.; Kelly, M. A.; Scharpen, L. H. *J. Appl. Polym. Sci.* **1978**, *22*, 643.

(32) Takahara, A.; Jo, N. J.; Kajiyama, T. *J. Biomater. Sci., Polym. Ed.* **1989**, *1*, 17.
(33) Takahara, A.; Korehisa, K.; Takahashi, K.; Kajiyama, T. *Kobunshi Ronbunshu* **1992**, *49*, 275.
(34) Takahara, A.; Takahashi, K.; Kajiyama, T. *J. Biomater. Sci., Polym. Ed.* **1993**, *5*, 183.
(35) Senshu, K.; Kobayashi, M.; Ikawa, N.; Yamashita, S.; Hirao, A.; Nakahama, S. *Langmuir* **1999**, *15*, 1763.
(36) Takahara, A.; Morotomi, N.; Hiraoka, S.; Higashi, N.; Kunitake, T.; Kajiyama, T. *Macromolecules* **1989**, *22*, 617.
(37) Volkov, V. V.; Plate, N. A.; Takahara, A.; Kajiyama, T.; Amaya, N.; Murata, Y. *Polymer* **1992**, *33*, 1316.
(38) Bunn, C. W.; Howells, E. R. *Nature* **1954**, *174*, 549.
(39) Corpart, J. M.; Girault, S.; Juhue′, D. *Langmuir* **2001**, *17*, 7237.
(40) Volkov, V. V.; Fadeev, A. G.; Plate, N. A.; Amaya, N.; Murata, Y.; Takahara, A.; Kajiyama, T. *Polym. Bull.* **1994**, *32*, 193.
(41) Furmidge, C. G. L. *J. Colloid Sci.* **1962**, *17*, 309.
(42) Miwa, M.; Nakajima, A.; Fujishima, A.; Hashimoto, K.; Watanabe, T. *Langmuir* **2000**, *16*, 5754.
(43) Oner, D.; McCarthy, T. J. *Langmuir* **2000**, *16*, 7777.
(44) Morita, M.; Koga, T.; Otsuka, H.; Takahara, A. *Langmuir* **2005**, *21*, 911.
(45) Fujimori, A.; Sugita, Y.; Nakahara, H.; Ito, E.; Hara, M.; Matsuie, N.; Kanai, K.; Ouchi, Y.; Seki, K. *Chem. Phys. Lett.* **2004**, *387*, 345.
(46) Lo, X.-D.; Aoki, A.; Miyashita, T. *Langmuir* **1996**, *12*, 5444.
(47) Hosemann, R. *Z. Phys.* **1950**, *128*, 1−35, 42.
(48) Lindenmeyer, P. H.; Hosemann, R. *J. Appl. Phys.* **1963**, *34*, 42.
(49) Hosemann, R.; Hindeleh, A. M. *J. Macromol. Sci., Phys.* **1995**, *B34*, 327.
(50) Rogers, S. S.; Mandelkern, L. *J. Phys. Chem.* **1957**, *61*, 985.